LANGMUIR
Article
Cite This: Langmuir 2018, 34, 12974−12981
pubs.acs.org/Langmuir

Molecular Dynamics Simulations of Surface and Interfacial Tension of Graft Polymer Melts

Michael Jacobs,[†] Heyi Liang,[†] Brandon Pugnet,[‡] and Andrey V. Dobrynin*[,†]

[†]Department of Polymer Science, University of Akron, Akron, Ohio 44325, United States
[‡]Department of Physics, Lafayette College, Easton, Pennsylvania 18045, United States

ABSTRACT: Understanding the surface properties of polymer melts is crucial for designing new polymeric coatings, adhesives, and composites. Here, we study the effect of molecular architecture on surface and interfacial tension of melts of graft and linear polymers by molecular dynamics simulations. In particular, we elucidate the effect of the degree of polymerization of the side chains n_{sc} and their grafting density $1/n_g$ on the surface tension of the graft polymer/vacuum interface, γ_G, and the interfacial tension of the interface between graft and linear polymer melts, γ_{GL}. For the case of the graft polymer/vacuum interface, our simulations confirm that the surface tension is a linear function of the fraction of the backbone ends f_{be} and side chain ends f_{se}, $\gamma_G = \gamma_\infty - \gamma_{be} f_{be} - \Delta\gamma f_{se}$, where γ_∞ is the surface tension of the system of graft polymers with infinite molecular weight and γ_{be} and $\Delta\gamma$ are surface tension contributions from backbone ends and difference between contributions coming from the side chain ends and grafting points, respectively. This dependence of the surface tension highlights the entropic origin of the surface tension corrections associated with the redistribution of the grafting points and ends at the interface. However, the interfacial tension of the interface between graft and linear polymer melts does not show any significant dependence on the molecular structure of the graft polymers, thus pointing out the dominance of enthalpic contribution to the interfacial tension.

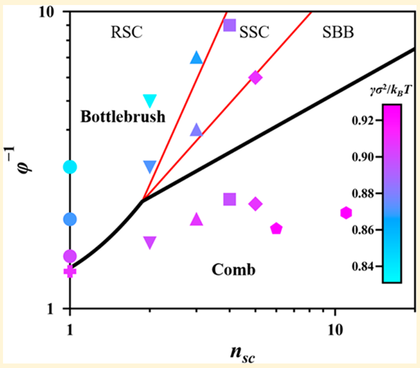

INTRODUCTION

Properties of graft polymers consisting of side chains attached to a polymer backbone are reflections of their molecular structure.[1−10] This unique chemical architecture allows for the control of the material properties at the synthesis stage. For example, independent variation in the side chain grafting density and their degree of polymerization (DP) results in effective disentanglement through the backbone dilution manifested in lower entanglement plateau shear modulus and zero shear viscosity.[1−9,11] This disentanglement feature of the graft polymers paved the way for computationally driven design of the solvent-free hyperelestic polymeric networks with modulus approaching that of gels and soft biological tissues.[12−17] Such networks were recently utilized to regulate a balance between elastic and capillary forces and to accurately map the entire range of particle−substrate interactions leading to the development of an approach for measuring the work of adhesion and surface tension of the elastic substrates.[18,19] Furthermore, the variation of the surface properties of the graft polymer melts and networks with the strand's molecular architecture is of paramount importance for improving these materials' adhesive and surface properties.

Chemical modifications of the graft polymers through attachment of the linear or graft chains to both ends of the graft polymers (ABA-type copolymers) led to a new class of thermoplastic materials (plastomers).[14,20,21] Under appropriate conditions, these macromolecules self-assemble forming composite materials consisting of glassy domains imbedded in the soft polymeric matrix of graft polymers. The spatial organization, symmetry, and size of the domains are a result of the fine interplay between the interfacial energy of the interface between A- and B-domains and the elastic energy of the graft polymer blocks' deformation. These composites have unique mechanical and optical properties depending on the special organization of the domains.[14] Therefore, to be able to predict what type of the domain structure one should expect for a particular ABA copolymer composition it is necessary to know the effect of the molecular architecture on the surface properties of the AB interface.

In this paper, to address the question of how the molecular architecture of the graft polymers influences their surface and interfacial properties, we performed coarse-grained molecular dynamics simulations of films of graft polymers in contact with a film of linear chains. The rest of the paper is organized as follows: (i) first we use classification of the graft polymers into combs and bottlebrushes to illustrate to what regime of the diagram of states the studied systems belong; (ii) then the effect of the ends and grafting points on the surface and interface properties is discussed; and (iii) finally, we establish dependence of the surface tension of the studied systems on the volume fraction of the ends and grafting points and compare it with existing models.[22−24]

Received: August 23, 2018
Revised: September 28, 2018
Published: October 17, 2018

DOI: 10.1021/acs.langmuir.8b02876
Langmuir 2018, 34, 12974−12981

MODEL AND SIMULATION DETAILS

We performed molecular dynamics simulations of films of the graft polymers having the DP of the backbone n_{bb}, DP of the side chains n_{sc}, and the number of bonds between neighboring side chains n_g (see Figure 1a)[16,25] in contact with a film of linear chains as shown in Figure 1b. The structural parameters of the studied systems are summarized in Table 1. Graft polymers and linear chains are modeled as bead-spring chains made of beads with diameter σ interacting through truncated-shifted Lennard-Jones (LJ) potential.

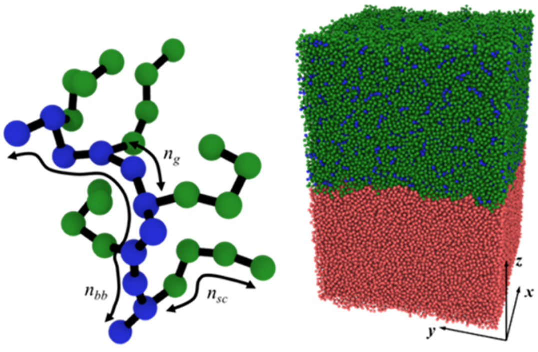

(a) (b)

Figure 1. (a) Graft polymer chain with the DP of the backbone n_{bb}, number of bonds between grafted side chains n_g, and DP of the side chains n_{sc}. Backbone and side chain monomers are shown as blue and green beads, respectively. (b) Snapshot of the simulation box showing films of graft polymers (top) and linear chains (bottom) in contact. System is periodic in x- and y-directions.

$$U_{\mathrm{LJ}}(r_{ij}) = \begin{cases} 4\varepsilon\left[\left(\dfrac{\sigma}{r_{ij}}\right)^{12} - \left(\dfrac{\sigma}{r_{ij}}\right)^{6} - \left(\dfrac{\sigma}{r_{\mathrm{cut}}}\right)^{12} + \left(\dfrac{\sigma}{r_{\mathrm{cut}}}\right)^{6}\right] & r_{ij} \le r_{\mathrm{cut}} \\ 0 & r_{ij} > r_{\mathrm{cut}} \end{cases} \quad (1)$$

The strength of the interaction potential is controlled by the LJ-interaction parameter ε. The value of the interaction parameter between monomers belonging to graft polymer chains was set to $\varepsilon_{\mathrm{GG}} = 1.0k_BT$ (where k_B is the Boltzmann constant and T is the absolute temperature), and for the monomers of linear chains it was $\varepsilon_{\mathrm{LL}} = 1.5k_BT$. We used the geometric mean approximation to calculate the interaction parameter between monomers belonging to graft polymers and linear chains, $\varepsilon_{\mathrm{GL}} = \sqrt{\varepsilon_{\mathrm{GG}}\varepsilon_{\mathrm{LL}}}$. The cutoff distance for pair-wise interactions was $r_{\mathrm{cut}} = 2.5\sigma$. The beads are connected to polymers by a bond potential which is modeled by a combination of the FENE and pure repulsive LJ-potentials. The repulsive part of the bond potential is described by the truncated-shifted LJ potential with $\varepsilon = 1.0k_BT$ and $r_{\mathrm{cut}} = 2^{1/6}\sigma$. In our simulations, we used the FENE potential

$$U_{\mathrm{FENE}}(r) = -\frac{1}{2}k_{\mathrm{spring}}R_{\mathrm{max}}^{\ 2}\ln\left(1 - \frac{r^2}{R_{\mathrm{max}}^{\ 2}}\right) \quad (2)$$

with the spring constant $k_{\mathrm{spring}} = 30k_BT/\sigma^2$ and the maximum bond length $R_{\mathrm{max}} = 1.5\sigma$.

Table 1. Summary of the Studied Systems

n_{bb}	n_g	n_{sc}	Total DP	Chain Ends	Graft Points	φ	Symbols used in Figures
32	32	0	32	2	0	1	⬢
28	28	0	28	2	0	1	⬟
24	24	0	24	2	0	1	◆
20	20	0	20	2	0	1	■
16	16	0	16	2	0	1	▲
12	12	0	12	2	0	1	▼
8	8	0	8	2	0	1	⬢
21	10	11	32	3	1	0.476	⬢
20	7	6	32	4	2	0.538	⬟
17	4	5	32	5	3	0.444	◆
16	3	4	32	6	4	0.429	■
17	3	3	32	7	5	0.5	▲
20	3	2	32	8	6	0.6	▼
24	3	1	32	10	8	0.75	✚
23	2	1	32	11	9	0.667	●
11	1	3	32	9	7	0.25	▲
12	1	2	32	12	10	0.333	▼
16	1	5	86	16	14	0.167	◆
17	1	1	32	17	15	0.5	●
18	1	1	32	16	14	0.5	●
19	1	1	32	15	13	0.5	●
20	1	1	32	14	12	0.5	●
21	1	1	32	13	11	0.5	●
8	0.5[a]	2	32	14	6	0.2	▼
12	0.5	1	32	22	10	0.3	●
20	0.5	1	56	38	18	0.3	●
20	0.5	2	92	38	18	0.2	▼
20	0.5	3	128	38	18	0.143	▲
20	0.5	4	164	38	18	0.111	■

[a] n_g = 0.5 corresponds to the systems with two side chains grafted to a monomer of the backbone.

Simulations were carried out in the canonical (NVT) ensemble. The constant temperature is maintained by coupling the system to a Langevin thermostat. In this case, the equation of motion of the ith bead is

$$m\frac{\mathrm{d}\vec{v}_i(t)}{\mathrm{d}t} = \vec{F}_i(t) - \xi\vec{v}_i(t) + \vec{F}_i^{\mathrm{R}}(t) \quad (3)$$

where m is the bead mass set to unity for all beads, $\vec{v}_i(t)$ is the bead velocity and $\vec{F}_i(t)$ is the net deterministic force acting on the ith bead. The stochastic force $\vec{F}_i^{\mathrm{R}}(t)$ acting on the ith bead has a zero average and δ-function correlation $\langle\vec{F}_i^{\mathrm{R}}(t)\cdot\vec{F}_j^{\mathrm{R}}(t')\rangle = 6k_BT\xi\delta_{ij}\delta(t - t')$. The friction coefficient ξ coupling a system to a Langevin thermostat was set to $\xi = 0.143m/\tau_{\mathrm{LJ}}$, where $\tau_{\mathrm{LJ}} = \sigma(m/k_BT)^{1/2}$ is the standard LJ time to maintain temperature $k_BT = 1.0$ in energetic units. The velocity-Verlet algorithm with time step $\Delta t = 0.005\tau_{\mathrm{LJ}}$ was used for integration of the equations of motion. All simulations were performed using LAMMPS[26] under two-dimensional periodic boundary conditions in the x and y directions (see Figure 1b).

All systems were prepared using the following procedure. First, polymers were randomly placed in a simulation box with dimensions $50.0\sigma \times 50.0\sigma \times 104.0\sigma$ to make the total number of monomers approximately 85 300. An initial simulation run of $2.0\tau_{\mathrm{LJ}}$ was carried out without pair-wise interactions to relax the initial chain conformations. The pair-wise interactions were

DOI: 10.1021/acs.langmuir.8b02876
Langmuir 2018, 34, 12974−12981

slowly turned on to full strength by performing a run lasting $26\tau_{LJ}$ with truncated-shifted LJ potential modified by a soft-core potential with the parameters $r_{cut} = 2.5\sigma$ and $\alpha = 0.5$ as implemented in LAMMPS[26]

$$U_{LJ}(r_{ij}) = \begin{cases} 4\delta^2\varepsilon\left(\left[\alpha(1-\delta)^2 + \left(\frac{r_{ij}}{\sigma}\right)^6\right]^{-2} - \left[\alpha(1-\delta)^2 + \left(\frac{r_{ij}}{\sigma}\right)^6\right]^{-1} - \left[\alpha(1-\delta)^2 + \left(\frac{r_{cut}}{\sigma}\right)^6\right]^{-2} + \left[\alpha(1-\delta)^2 + \left(\frac{r_{cut}}{\sigma}\right)^6\right]^{-1}\right) & r_{ij} \le r_{cut} \\ 0 & r_{ij} > r_{cut} \end{cases} \quad (4)$$

During this simulation run, the parameter δ, describing the weight of the LJ-potential in the soft-core potential was increased from 0.1 to 1.0 with an increment of 0.1. Note that the soft-core interaction potential prevents the divergence of forces acting on the beads during the system preparation step and recovers the LJ-potential as δ becomes 1.0. A simulation run of $710\tau_{LJ}$ was then carried out using the truncated-shifted LJ-potential (eq 1). These preparatory steps were completed for each of the graft polymer films and for the films of linear polymers.

Once the preparation steps were completed, a film of the linear polymers was placed under the film of graft polymers. An attractive harmonic potential with spring constant $K = 0.5k_BT\sigma^{-2}$ was imposed on the center of masses of the film of graft polymers and of the film of linear chains. These simulations were continued for $250\tau_{LJ}$, then harmonic potential was removed and a run of $500\tau_{LJ}$ was performed to relax the interface. Next, a simulation run of $5 \times 10^4\tau_{LJ}$ was carried out to insure that the radius of gyration of the chains reached equilibrium (saturated as a function of time). After equilibration was complete, a simulation run of $5 \times 10^4\tau_{LJ}$ was performed for the data collection.

■ RESULTS AND DISCUSSION

Diagram of States. The molecular architecture of the graft polymers is described in terms of the graft polymer composition

$$\varphi = \frac{n_g}{n_g + n_{sc}} \quad (5)$$

characterizing the volume fraction of the backbone monomers and the DP of the side chains, n_{sc}. Our classification of the graft polymers into combs and bottlebrushes in a melt is based on the degree of mutual interpenetration of the side chains belonging to neighboring graft macromolecules.[25] This is quantified by the value of the crowding parameter, Φ, defined as a ratio of the volume occupied by monomers of the given graft macromolecule within the pervaded volume of chains of blobs, each with the size of a side chain (see ref 25 for details). For combs, the value of the crowding parameter is $\Phi < 1$, whereas for bottlebrushes, it is $\Phi > 1$. Computer simulations of the graft polymer melts show that the crossover from combs to bottlebrushes takes place when the value of the crowding parameter is on the order of $\Phi \approx 0.7$.[25] Using the expressions for the crowding parameter in terms of the monomer excluded volume v, bond length l, and Kuhn length b, we obtain an expression defining the crossover line for graft polymers with flexible (long) side chains ($n_{sc} \ge b/l$)

$$\Phi \approx \frac{v}{(lb)^{3/2}}\varphi^{-1}n_{sc}^{-1/2} \approx 0.7 \Rightarrow \varphi^{-1} \approx 0.7\rho(lb)^{3/2}n_{sc}^{1/2} \quad (6)$$

and with rod-like (short) side chains ($n_{sc} < b/l$)

$$\Phi \approx \frac{v}{l^3}\varphi^{-1}n_{sc}^{-2} \approx 0.7 \Rightarrow \varphi^{-1} \approx 0.7\rho l^3 n_{sc}^{2} \quad (7)$$

In rewriting eqs 6 and 7, we estimated the excluded volume from the monomer density $v = \rho^{-1}$. Note that for our set of parameters, defining interaction and bonding potentials, the excluded volume, $v = \rho^{-1} = 1.024\sigma^3$, bond length $l = 0.985\sigma$, and the Kuhn length $b = 1.845\sigma$ were calculated from the bond–bond correlation function in the melt of linear chains.[25]

The diagram of states of graft polymers in terms of φ^{-1} and DP of the side chains, n_{sc}, is shown in Figure 2. The crossover lines described by eqs 6 and 7 are shown as a thick solid line. Below, we briefly overview the main features of the graft polymers in *Comb* and *Bottlebrush* regimes.[25] In the *Comb* regime, both side chains and backbones of graft polymers interpenetrate and remain in their unperturbed ideal chain conformations such that the effective Kuhn length of combs is equal to that of the linear chains ($b_K \cong b$). In the *Bottlebrush* regime, the excluded volume interactions between side chains result in (i) withdrawal of its side chains from neighboring macromolecules, (ii) extension of the backbone and side chains, and (iii) stiffening of a graft macromolecule ($b_K > b$). Because of the changes in conformations of the side chains and backbone, there are three sub-regimes in the *Bottlebrush* regime. Bottlebrushes with extended backbones belong to the

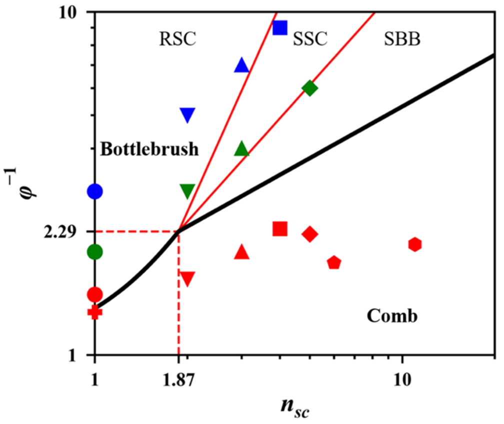

Figure 2. Diagram of states of graft polymers. The solid black line corresponds to a crossover between *Comb* and *Bottlebrush* regimes and is calculated using eq 6 for flexible side chains. In this calculation, we used $l = 0.985\sigma$, $b = 1.845\sigma$, and $v = \rho^{-1} = 1.024\sigma^3$. The location of the intersection point is obtained by substituting $n_{sc} = b/l = 1.873$ into the expression for φ^{-1} at the crossover between *Comb* and *Bottlebrush* regimes: $\varphi^{-1} \approx 0.7\rho b^2 l \approx 2.29$. The boundary between *Comb* and *Bottlebrush* regimes for rod-like side chains $n_{sc} < 1.873$ is given by $\varphi^{-1} = 1 + 0.368\rho l^3 n_{sc}^2$, which goes through points with coordinates (0, 1) and (1.873, 2.29). The crossover between SBB and SSC sub-regimes is given by $\varphi^{-1} \approx 0.7\rho b l^2 n_{sc}$, whereas for the crossover SSC/RSC, we used $\varphi^{-1} \approx 0.7\rho l^3 n_{sc}^2$ (see ref 25). See Table 1 for symbol notations.

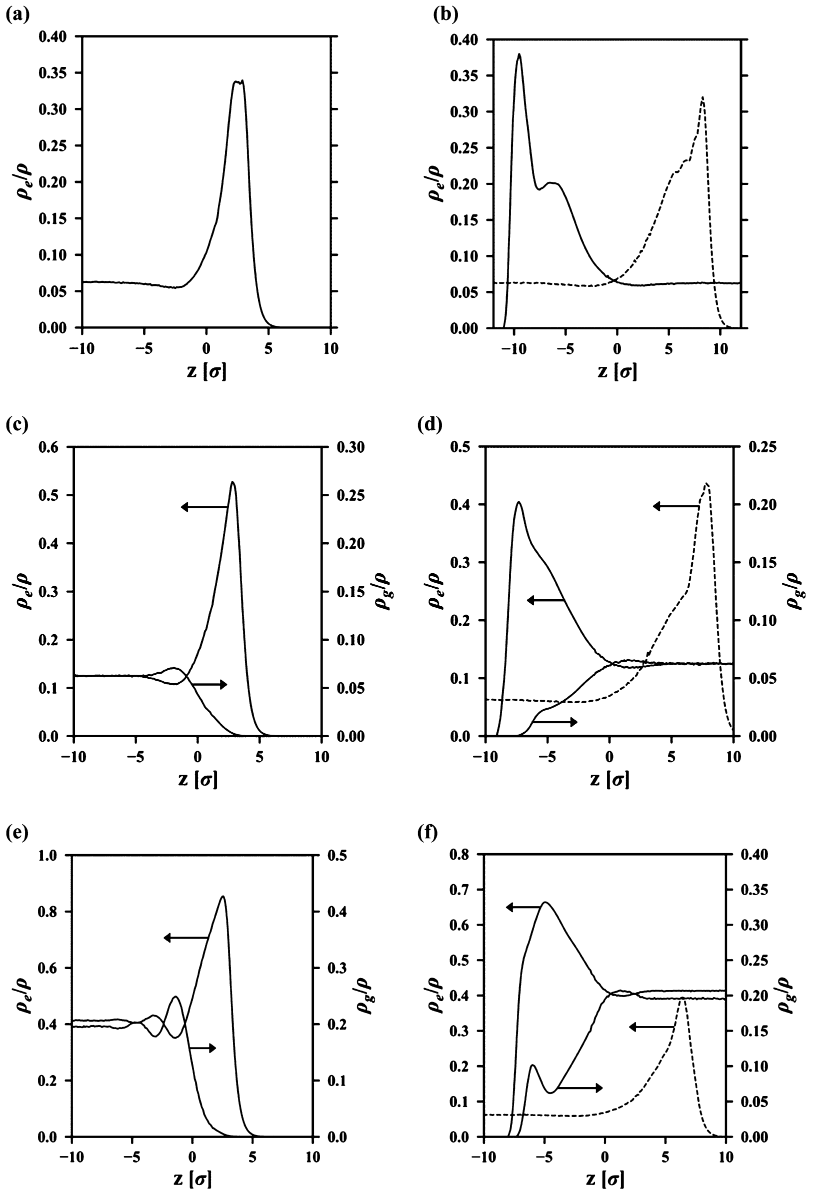

Figure 3. Normalized density distribution of the ends and grafting points across the interface. (a) Interface of vacuum and melt of linear chains with $N = 32$. (b) Interface between melts of linear chains with $N = 32$. (c) Interface of vacuum and melt of combs with $n_{bb} = 23$, $n_g = 7$, $n_{sc} = 6$. (d) Interface between melt of combs with $n_{bb} = 23$, $n_g = 7$, and $n_{sc} = 6$ and melt of linear chains with $N = 32$. (e) Interface of vacuum and melt of bottlebrushes with $n_{bb} = 20$, $n_g = 0.5$, and $n_{sc} = 2$. (f) Interface between melt of bottlebrushes with $n_{bb} = 20$, $n_g = 0.5$, and $n_{sc} = 2$ and melt of linear chains with $N = 32$. Location with $z = 0$ corresponds to a half of the monomer bulk density for polymer/vacuum interfaces and to a point of equal monomer density of corresponding components for the interface between two melts.

Stretched Backbone (SBB) sub-regime, whereas those with stretched side chains are within the Stretched Side Chain (SSC) sub-regime. Bottlebrushes with fully stretched side chains belong to the Rod-like Side Chain (RSC) sub-regime. The crossover lines between different sub-regimes are shown as red lines in Figure 2. The points in this diagram of states correspond to studied graft polymer systems listed in Table 1. It is important to point out that the graft polymer with side chain $n_{sc} = 1$ represents an extreme case of graft polymers with rod-like side chains. This type of graft polymer has the largest fraction of the ends per backbone monomer among all graft polymers with the same value of n_g. Thus, the selected range of architectural parameters of graft polymers covers both *Comb* and *Bottlebrush* regimes. In the next section, we describe surface and interfacial properties of these graft polymers in a melt.

Surface and Interface Properties. Figure 3 shows the end and grafting point density of six systems as a function of the *z*-coordinate near the vacuum interface and the interface between melts of graft and linear polymers. To highlight surface affinity between the ends and grafting points and the interface, we have normalized the corresponding density functions $\rho_i(z)$ by the total monomer density $\rho(z)$. Note that in the bulk, these normalized densities saturate at values corresponding to the ratio of the number of ends or grafting points to the total number of monomers per graft polymer or linear chain. As evident from all plots in Figure 3, the ends are attracted to the interface, which is manifested by the broad peaks. The distribution function of ends for linear chains and combs look qualitatively similar (panels a–d). The main difference between combs and linear chains is the appearance of the peaks corresponding to the accumulation of the grafting points at the interface. This feature becomes more pronounced for bottlebrush systems (panels e and f) where we see multiple peaks for the distribution functions of both ends and grafting points. These peaks are out of phase indicating an effective “polarization” of the ends and grafting points close to the interface. It is important to point out that, in the case of density distribution across the interface between melts of the graft polymers and linear chains, the peaks appear to be broader for both comb and bottlebrush systems (panels b, d, and f).

Changes in the density distribution of the ends and grafting points influence the surface tension of the interface. To establish this correlation, we have calculated the surface and interfacial tension for all studied systems. In simulations, the surface tension is obtained from integration across the interface of the pressure difference $\Delta P = P_n - P_t$ between the normal P_n and transversal P_t to the interface pressure tensor components.[27] These components are expressed in terms of the diagonal pressure tensor components (P_{xx}, P_{yy}, P_{zz}) as follows $P_t = (P_{xx} + P_{yy})/2$ and $P_n = P_{zz}$. Figure 4 illustrates distribution of the time averaged pressure difference ΔP across the film thickness. This function has nonzero values in the interface regions, whereas it fluctuates around zero in the film bulk. Integration of this function across the interface region provides the value of the surface tension for the graft polymer/vacuum, graft polymer/linear polymer, and linear polymer/vacuum interfaces. For example, in the case of the i-th interface the integration is performed between left $z = \xi_{i,l}$ and right $z = \xi_{i,r}$ integration boundary

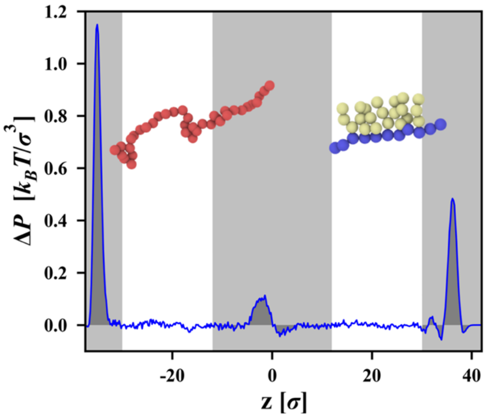

Figure 4. Typical time averaged pressure difference profile for a bottlebrush system with $n_g = 0.5$ and $n_{sc} = 3$. Integration intervals used for calculations of the surface tension are highlighted in gray. Insets show the type of macromolecule the films are made of.

$$\gamma_i = \int_{\xi_{i,l}}^{\xi_{i,r}} \left[P_{zz}(z) - \frac{1}{2}(P_{xx}(z) + P_{yy}(z)) \right] dz \tag{8}$$

The results of these calculations are presented in Figure 5. In particular, Figure 5a shows surface tension for the graft chain/linear chain interface as a function of the fraction of the ends. As shown in this figure, γ_{GL} has no discernible trend, with all values falling within the 0.22–0.26$k_BT\sigma^{-2}$ interval. Thus, the variation in the chemical structure of the graft polymer chains does not have a well-established trend on the surface tension. This indicates that the surface tension is dominated by interactions between monomers rather than redistribution of the ends and grafting points. The surface tension of the vacuum interface, however, shows a much more peculiar behavior (see Figure 5b). First, there is a general trend of decrease in the surface tension with increasing fraction of the ends. This type of behavior is expected for systems of linear chains. In addition to this linear decrease, we also have several saturation levels illustrated by the dashed lines which correspond to combs and bottlebrushes, belonging to different regimes of the diagram of state. This peculiar behavior of the surface tension is a reflection of the changes in the corresponding density profiles (see Figure 3).

The calculations in the framework of the linear response approximation[22−24] and self-consistent field calculations[23,24,28] have shown that the surface tension of the branched polymers is a linear function of the fraction of ends and branching points. This was confirmed for systems of linear polymers,[29−34] branched polymers of different molecular architectures,[24,35,36] and polymer-grafted nanoparticles.[37] Our case of the graft polymers is a special case of the branched polymers for which the number of branching points is equal to the number of the side chains or double this number per graft polymer. Thus for systems with $n_g \geq 1$, there are two ends per backbone and the number n_{gr} of grafted side chains is equal to the number of grafting points and to the number of side chain ends. We can define the fraction of the backbone ends, f_{be}, side chain ends, f_{se}, and grafting points, f_{gr}, as follows

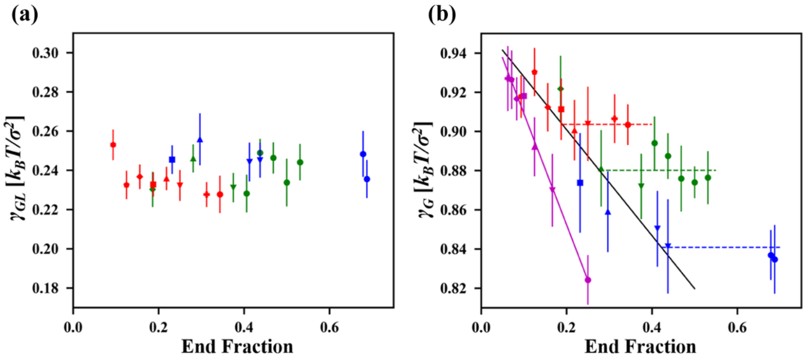

Figure 5. Dependence of surface tension of the melt of graft chains on the end fraction of the graft polymers for the interface with the melt of linear chains (a) and with the vacuum (b). Symbol notations are the same as in Table 1.

$$f_{\mathrm{be}} = 2/N, \qquad f_{\mathrm{se}} = f_{\mathrm{gr}} = n_{\mathrm{gr}}/N \qquad \text{for } n_{\mathrm{g}} \geq 1 \tag{9}$$

where the total number of monomers in a graft macromolecule is equal to $N = n_{\mathrm{bb}} + n_{\mathrm{sc}}n_{\mathrm{gr}}$. In the case when there are two side chains grafted to the same grafting points, the fraction of the backbone ends, side chain ends, and grafting points is equal to

$$f_{\mathrm{be}} = 2/N, \qquad f_{\mathrm{se}} = 2f_{\mathrm{gr}} = n_{\mathrm{gr}}/N \qquad \text{for } n_{\mathrm{g}} = 0.5 \tag{10}$$

The surface tension of the graft polymer/vacuum interface is written as[22−24]

$$\gamma_{\mathrm{G}} = \gamma_{\infty} - \gamma_{\mathrm{be}}f_{\mathrm{be}} - \gamma_{\mathrm{se}}f_{\mathrm{se}} + \gamma_{\mathrm{g}}f_{\mathrm{gr}} \tag{11}$$

where γ_{∞} is the surface tension of the system of graft polymers with infinite molecular weight, γ_{be}, γ_{se}, and γ_{g} are surface tension contributions from backbone ends, side chain ends, and grafting points, respectively. Since, for our graft polymers, there is a linear relationship between the fraction of side chain ends and grafting points, we will only be able to find a difference in contributions from the side chain ends and grafting points to the surface tension

$$\gamma_{\mathrm{G}} = \gamma_{\infty} - \gamma_{\mathrm{be}}f_{\mathrm{be}} - \Delta\gamma f_{\mathrm{se}} \tag{12}$$

where $\Delta\gamma = \gamma_{\mathrm{se}} - \gamma_{\mathrm{g}}$ for $n_{\mathrm{g}} \geq 1$ and $\Delta\gamma = \gamma_{\mathrm{se}} - \gamma_{\mathrm{g}}/2$ for $n_{\mathrm{g}} = 0.5$. Note that this dependence of the surface tension of graft polymers is a manifestation of the redistribution of the ends and grafting points and thus entropic in origin.[22−24]

Figure 6 shows a three-dimensional (3-D) plot of the surface tension dependence as a function of the fraction of backbone and side chain ends for all our studied systems. Analysis of the data shows that we have to separate systems with $n_{\mathrm{g}} \geq 1$ and $n_{\mathrm{g}} = 0.5$. By fitting together the data for $n_{\mathrm{g}} \geq 1$ to eq 12, we find that $\gamma_{\infty} = 0.96k_{\mathrm{B}}T/\sigma^2$, $\gamma_{\mathrm{be}} = 0.55k_{\mathrm{B}}T/\sigma^2$, and $\Delta\gamma = 0.12k_{\mathrm{B}}T/\sigma^2$. As evident from the fitting results, the data for $n_{\mathrm{g}} = 0.5$ systems are outside the confidence level for the best fit plot. The analysis of the data set for $n_{\mathrm{g}} = 0.5$ with a fixed $\gamma_{\mathrm{be}} = 0.55\ k_{\mathrm{B}}T/\sigma^2$ gives $\gamma_{\infty} = 0.88k_{\mathrm{B}}T/\sigma^2$ and $\Delta\gamma = 0.032k_{\mathrm{B}}T/\sigma^2$. The difference between fitting parameters indicates that there is a difference in parameter γ_{g} depending on the number of grafted chains per backbone monomer which is manifested in the smaller value of $\Delta\gamma = 0.032k_{\mathrm{B}}T/\sigma^2$ for systems with $n_{\mathrm{g}} = 0.5$. This points out the breakdown of the simple addition approximation for contribution of the number of grafted side chains into γ_{g}.

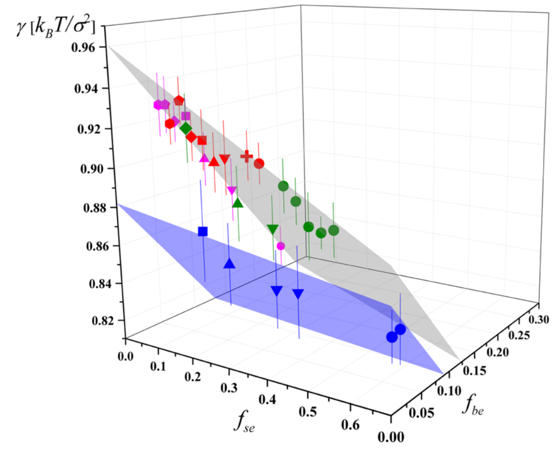

Figure 6. Dependence of the surface tension γ of the melt of graft chains on the fraction of backbone chain ends f_{be} and the fraction of the side chain ends f_{se}. The blue plane is the best fit for densely grafted bottlebrushes with $n_{\mathrm{g}} = 0.5$. The gray plane is the best fit for systems with $n_{\mathrm{g}} \geq 1$. Symbol notations are the same as in Table 1.

CONCLUSIONS

We have presented results of the molecular dynamics simulations of the surface properties of graft polymers as a function of their molecular architecture. Analysis of the simulation data confirms a linear relationship between surface tension of the graft polymer melt/vacuum interface and the fraction of the backbone and side chain ends for systems with side chain grafting density $n_{\mathrm{g}}^{-1} \leq 1$. In particular, we show that it is more convenient to plot data in 3-D representation (see Figure 6). However, for systems with $n_{\mathrm{g}} = 0.5$, the values of the fitting parameters are different from those for systems with $n_{\mathrm{g}} \geq 1$, indicating additional corrections to parameter γ_{g} because of packing restrictions of the grafting points with four bonds connected to the grafting point. Thus for densely grafted side chains, there are strong correlation effects in distributions of the side chains close to the grafting points which could be responsible for the observed trend.

In Figure 7, we have combined our simulation results for the graft polymer/vacuum interface into the diagram of states. This data representation highlights that the lowest surface tension is observed for the films of bottlebrushes with the highest density of the ends per macromolecule. The surface tension gradually increases toward the region of the diagram of states corresponding to combs with loosely grafted long side chains. Such systems are characterized by low fraction of the ends and thus higher surface tension but still being smaller than that of the linear chains with the same total DP. These results provide confirmation for the surface affinity of graft polymers and their segregation at the interface in mixtures of linear and graft polymers.[38−40]

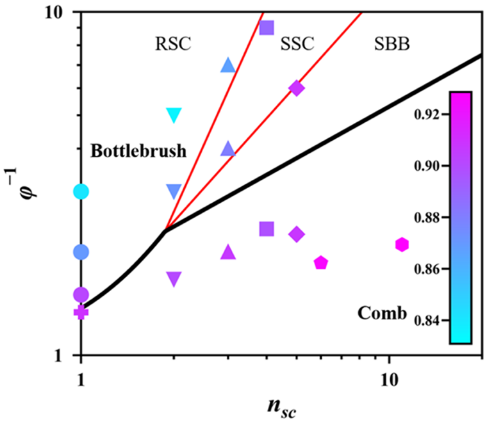

Figure 7. Diagram of states of graft polymers and surface tension of the graft polymer melt/vacuum interface shown by different point colors. The surface tension scale is in $k_{\mathrm{B}}T/\sigma^2$ units. The solid black line corresponds to a crossover between *Comb* and *Bottlebrush* regimes.

The strong effect of the molecular architecture of the graft polymers on the interfacial properties disappears in the case of the interface between melts of linear and graft polymers (Figure 5a). This points out the enthalpic origin of the interfacial tension which is dominated by the interactions rather than by the entropy change because of redistribution of the grafting points and ends.

■ AUTHOR INFORMATION

Corresponding Author

*E-mail: adobrynin@uakron.edu.

ORCID

Heyi Liang: 0000-0002-8308-3547

Andrey V. Dobrynin: 0000-0002-6484-7409

Funding

National Science Foundation (DMR-1624569).

Notes

The authors declare no competing financial interest.

■ REFERENCES

(1) Fetters, L. J.; Lohse, D. J.; García-Franco, C. A.; Brant, P.; Richter, D. Prediction of Melt State Poly(α-olefin) Rheological Properties: The Unsuspected Role of the Average Molecular Weight per Backbone Bond. *Macromolecules* **2002**, *35*, 10096−10101.

(2) Hadjichristidis, N.; Xenidou, M.; Iatrou, H.; Pitsikalis, M.; Poulos, Y.; Avgeropoulos, A.; Sioula, S.; Paraskeva, S.; Velis, G.; Lohse, D. J.; Schulz, D. N.; Fetters, L. J.; Wright, P. J.; Mendelson, R. A.; García-Franco, C. A.; Sun, T.; Ruff, C. J. Well-Defined, Model Long Chain Branched Polyethylene. 1. Synthesis and Characterization. *Macromolecules* **2000**, *33*, 2424−2436.

(3) Lohse, D. J.; Milner, S. T.; Fetters, L. J.; Xenidou, M.; Hadjichristidis, N.; Mendelson, R. A.; García-Franco, C. A.; Lyon, M. K. Well-Defined, Model Long Chain Branched Polyethylene. 2. Melt Rheological Behavior. *Macromolecules* **2002**, *35*, 3066−3075.

(4) Dalsin, S. J.; Hillmyer, M. A.; Bates, F. S. Linear Rheology of Polyolefin-Based Bottlebrush Polymers. *Macromolecules* **2015**, *48*, 4680−4691.

(5) Daniels, D. R.; McLeish, T. C. B.; Crosby, B. J.; Young, R. N.; Fernyhough, C. M. Molecular Rheology of Comb Polymer Melts. 1. Linear Viscoelastic Response. *Macromolecules* **2001**, *34*, 7025−7033.

(6) Hu, M.; Xia, Y.; McKenna, G. B.; Kornfield, J. A.; Grubbs, R. H. Linear Rheological Response of a Series of Densely Branched Brush Polymers. *Macromolecules* **2011**, *44*, 6935−6943.

(7) Daniel, W. F. M.; Burdyńska, J.; Vatankhah-Varnoosfaderani, M.; Matyjaszewski, K.; Paturej, J.; Rubinstein, M.; Dobrynin, A. V.; Sheiko, S. S. Solvent-Free, Supersoft and Superelastic Bottlebrush Melts and Networks. *Nat. Mater.* **2016**, *15*, 183−189.

(8) Matyjaszewski, K.; Tsarevsky, N. V. Macromolecular Engineering by Atom Transfer Radical Polymerization. *J. Am. Chem. Soc.* **2014**, *136*, 6513−6533.

(9) Abbasi, M.; Faust, L.; Riazi, K.; Wilhelm, M. Linear and Extensional Rheology of Model Branched Polystyrenes: From Loosely Grafted Combs to Bottlebrushes. *Macromolecules* **2017**, *50*, 5964−5977.

(10) Uhrig, D.; Mays, J. W. Synthesis of Combs, Centipedes, and Barbwires: Poly(isoprene-graft-styrene) Regular Multigraft Copolymers with Trifunctional, Tetrafunctional, and Hexafunctional Branch Points. *Macromolecules* **2002**, *35*, 7182−7190.

(11) Haugan, I. N.; Maher, M. J.; Chang, A. B.; Lin, T.-P.; Grubbs, R. H.; Hillmyer, M. A.; Bates, F. S. Consequences of Grafting Density on the Linear Viscoelastic Behavior of Graft Polymers. *ACS Macro Lett.* **2018**, *7*, 525−530.

(12) Vatankhah-Varnoosfaderani, M.; Daniel, W. F. M.; Zhushma, A. P.; Li, Q.; Morgan, B. J.; Matyjaszewski, K.; Armstrong, D. P.; Spontak, R. J.; Dobrynin, A. V.; Sheiko, S. S. A New Platform for Freestanding Electroactuation. *Adv. Mater.* **2017**, *29*, 1604209.

(13) Vatankhah-Varnosfaderani, M.; Daniel, W. F. M.; Everhart, M. H.; Pandya, A. A.; Liang, H.; Matyjaszewski, K.; Dobrynin, A. V.; Sheiko, S. S. Mimicking Biological Stress-Strain Behavior with Synthetic Elastomers. *Nature* **2017**, *549*, 497−501.

(14) Vatankhah-Varnosfaderani, M.; Keith, A. N.; Cong, Y.; Liang, H.; Rosenthal, M.; Sztucki, M.; Clair, C.; Magonov, S.; Ivanov, D. A.; Dobrynin, A. V.; Sheiko, S. S. Chameleon-Like Elastomers with Molecularly Encoded Strain-Adaptive Stiffening and Coloration. *Science* **2018**, *359*, 1509−1513.

(15) Sheiko, S. S.; Everhart, M. H.; Dobrynin, A. V.; Vatankhah-Varnosfaderani, M. Encoding Tissue Mechanics in Silicone. *Sci. Robot.* **2018**, *3*, No. eaat7175.

(16) Cao, Z.; Carrillo, J.-M. Y.; Sheiko, S. S.; Dobrynin, A. V. Computer Simulations of Bottle Brushes: From Melts to Soft Networks. *Macromolecules* **2015**, *48*, 5006−5015.

(17) Cao, Z.; Daniel, W. F. M.; Vatankhah-Varnosfaderani, M.; Sheiko, S. S.; Dobrynin, A. V. Dynamics of Bottlebrush Networks. *Macromolecules* **2016**, *49*, 8009−8017.

(18) Ina, M.; Cao, Z.; Vatankhah-Varnoosfaderani, M.; Everhart, M. H.; Daniel, W. F. M.; Dobrynin, A. V.; Sheiko, S. S. From Adhesion to Wetting: Contact Mechanics at the Surfaces of Super-Soft Brush-Like Elastomers. *ACS Macro Lett.* **2017**, *6*, 854−858.

(19) Tian, Y.; Ina, M.; Cao, Z.; Sheiko, S. S.; Dobrynin, A. V. How To Measure Work of Adhesion and Surface Tension of Soft Polymeric Materials. *Macromolecules* **2018**, *51*, 4059−4067.

(20) Zhang, J.; Schneiderman, D. K.; Li, T.; Hillmyer, M. A.; Bates, F. S. Design of Graft Block Polymer Thermoplastics. *Macromolecules* **2016**, *49*, 9108−9118.

(21) Verduzco, R.; Li, X.; Pesek, S. L.; Stein, G. E. Structure, Function, Self-Assembly, and Applications of Bottlebrush Copolymers. *Chem. Soc. Rev.* **2015**, *44*, 2405−2420.

(22) Wu, D. T.; Fredrickson, G. H. Effect of Architecture in the Surface Segregation of Polymer Blends. *Macromolecules* **1996**, *29*, 7919−7930.

(23) Minnikanti, V. S.; Archer, L. A. Surface Enrichment of Branched Polymers in Linear Hosts: Effect of Asymmetry in Intersegmental Interactions and Density Gradients. *J. Chem. Phys.* **2005**, *122*, 084904.

(24) Minnikanti, V. S.; Archer, L. A. Entropic Attraction of Polymers toward Surfaces and Its Relationship to Surface Tension. *Macromolecules* **2006**, *39*, 7718−7728.

(25) Liang, H.; Cao, Z.; Wang, Z.; Sheiko, S. S.; Dobrynin, A. V. Combs and Bottlebrushes in a Melt. *Macromolecules* **2017**, *50*, 3430−3437.

(26) Plimpton, S. Fast Parallel Algorithms for Short-Range Molecular Dynamics. *J. Comp. Physiol.* **1995**, *117*, 1−19.

(27) Rowlinson, J. S.; Widom, B. *Molecular Theory of Capillarity*; Clarendon Press: Oxford, 1982.

(28) Balazs, A. C.; Gersappe, D.; Israels, R.; Fasolka, M. Using Monte Carlo Simulations and Self-Consistent Field Theory to Design Interfacially Active Copolymers. *Macromol. Theory Simul.* **1995**, *4*, 585−612.

(29) Retsos, H.; Margiolaki, I.; Messaritaki, A.; Anastasiadis, S. H. Interfacial Tension in Binary Polymer Blends in the Presence of Block Copolymers: Effects of Additive MW. *Macromolecules* **2001**, *34*, 5295−5305.

(30) Jalbert, C.; Koberstein, J. T.; Yilgor, I.; Gallagher, P.; Krukonis, V. Molecular Weight Dependence and End-Group Effects on the Surface Tension of Poly(dimethylsiloxane). *Macromolecules* **1993**, *26*, 3069−3074.

(31) Jalbert, C.; Koberstein, J. T.; Hariharan, A.; Kumar, S. K. End Group Effects on Surface Properties of Polymers: Semiempirical Calculations and Comparison to Experimental Surface Tensions for α, ω-Functional Poly(dimethylsiloxanes). *Macromolecules* **1997**, *30*, 4481−4490.

(32) Genzer, J.; Composto, R. J. Effect of Molecular Weight on the Interfacial Excess, Tension, and Width in a Homopolymer/Binary Polymer Blend System. *Macromolecules* **1998**, *31*, 870−878.

(33) Fleischer, C. A.; Koberstein, J. T.; Krukonis, V.; Wetmore, P. A. The Effect of End Groups on Thermodynamics of Immiscible Polymer Blends. 1. Interfacial Tension. *Macromolecules* **1993**, *26*, 4172−4178.

(34) Dee, G. T.; Sauer, B. B. The Molecular Weight and Temperature Dependence of Polymer Surface Tension: Comparison

of Experiment with Interface Gradient Theory. *J. Colloid Interface Sci.* **1992**, *152*, 85−103.

(35) Retsos, H.; Anastasiadis, S. H.; Pispas, S.; Mays, J. W.; Hadjichristidis, N. Interfacial Tension in Binary Polymer Blends in the Presence of Block Copolymers. 2. Effects of Additive Architecture and Composition. *Macromolecules* **2004**, *37*, 524−537.

(36) Qian, Z.; Minnikanti, V. S.; Sauer, B. B.; Dee, G. T.; Archer, L. A. Surface Tension of Symmetric Star Polymer Melts. *Macromolecules* **2008**, *41*, 5007−5013.

(37) Che, J.; Jawaid, A.; Grabowski, C. A.; Yi, Y.-J.; Louis, G. C.; Ramakrishnan, S.; Vaia, R. A. Stability of Polymer Grafted Nanoparticle Monolayers: Impact of Architecture and Polymer−Substrate Interactions on Dewetting. *ACS Macro Lett.* **2016**, *5*, 1369−1374.

(38) Yethiraj, A. Entropic and Enthalpic Surface Segregation from Blends of Branched and Linear Polymers. *Phys. Rev. Lett.* **1995**, *74*, 2018−2021.

(39) Lee, J. S.; Lee, N.-H.; Peri, S.; Foster, M. D.; Majkrzak, C. F.; Hu, R.; Wu, D. T. Surface Segregation Driven by Molecular Architecture Asymmetry in Polymer Blends. *Phys. Rev. Lett.* **2014**, *113*, 225702.

(40) Mitra, I.; Li, X.; Pesek, S. L.; Makarenko, B.; Lokitz, B. S.; Uhrig, D.; Ankner, J. F.; Verduzco, R.; Stein, G. E. Thin Film Phase Behavior of Bottlebrush/Linear Polymer Blends. *Macromolecules* **2014**, *47*, 5269−5276.